JVST B
Journal of Vacuum Science & Technology B

Individual arc-discharge synthesized multiwalled carbon nanotubes probed with multiple measurement techniques

Cite as: J. Vac. Sci. Technol. B **38**, 042804 (2020); https://doi.org/10.1116/6.0000187
Submitted: 12 March 2020 . Accepted: 10 June 2020 . Published Online: 29 June 2020

Markus Ahlskog, Matti J. Hokkanen, Dmitry Levshov, Krister Svensson, Alexander Volodin, and Chris van Haesendonck

JVST B
Journal of Vacuum Science & Technology B

ARTICLE

avs.scitation.org/journal/jvb

Individual arc-discharge synthesized multiwalled carbon nanotubes probed with multiple measurement techniques

Cite as: J. Vac. Sci. Technol. B 38, 042804 (2020); doi: 10.1116/6.0000187
Submitted: 12 March 2020 · Accepted: 10 June 2020 ·
Published Online: 29 June 2020

Markus Ahlskog,[1,a)] Matti J. Hokkanen,[1,b)] Dmitry Levshov,[2,c)] Krister Svensson,[3] Alexander Volodin,[4] and Chris van Haesendonck[4]

AFFILIATIONS

[1]Department of Physics and Nanoscience Center, University of Jyvaskyla, Jyvaskyla, Karlstad, Espoo FI-40014, Finland
[2]Faculty of Physics, Southern Federal University, 5 Zorge Street, Rostov-on-Don 344090, Russia
[3]Department of Engineering and Physics, Karlstad University, Karlstad SE-65188, Sweden
[4]Department of Physics and Astronomy, KU Leuven, Celestijnenlaan 200 D, 3001 Leuven, Belgium

[a)]**Electronic mail:** markus.e.ahlskog@jyu.fi
[b)]**Present address:** School of Electrical Engineering and Automation, Aalto University, Espoo FI-00076, Finland.
[c)]**Present address:** Physics Department, University of Antwerp, Universiteitsplein 1, B-2610 Antwerp, Belgium.

ABSTRACT

Arc-discharge synthesized multiwalled carbon nanotubes (AD-MWNT), or related MWNTs, exhibit a good quality compared to the more common type of MWNT synthesized by catalytic chemical vapor deposition methods. Yet experimental measurements on these are rather few and typically have not correlated data from different measurement techniques. Here, the authors report Raman spectroscopy, scanning probe microscopy, conductivity measurements, and force microscopy on single AD-MWNTs. The results demonstrate the high quality of AD-MWNTs and are compatible with the view of them as the best approximation of MWNTs as an assembly of defect-free concentric individual single-walled carbon nanotubes. The authors also demonstrate conductance measurements over a step on the surface of an AD-MWNT, which is due to an abruptly broken outer layer(s), whereby the interlayer resistance is measured.

I. INTRODUCTION

The first carbon nanotubes studied in the pioneering work of Iijima in the early 1990s[1] were multiwalled carbon nanotubes (MWNT) synthesized by the arc-discharge method (AD-MWNT). These were soon accompanied by single-walled carbon nanotubes (SWNTs), on which most of the worldwide research interest has mostly been directed. Among MWNTs in general, those synthesized catalytically by CVD methods ("CCVD-tubes") have attracted much more interest than AD-MWNTs due to the fact that their fabrication is relatively easy to scale up,[2] while the arc-discharge method conveniently produces only laboratory scale amounts. Moreover, AD-MWNT material is, due to the synthesis method, severely intermixed with amorphous carbon material, the removal of which usually brings degradation of the AD-MWNTs.[3,4] Due to these circumstances, there are still relatively few thorough works on the properties of the AD-MWNTs. The difference to CCVD-tubes has partly been staked out, though not systematically. First, it is usually very apparent: AD-MWNTs have a straight geometry as opposed to the intrinsically curved CCVDs. It has been shown that AD-MWNTs have a much higher Young's modulus than CCVDs.[5,6] Raman spectra in CCVDs exhibit a strong defect-induced D-band, which is weak or negligible in AD-MWNTs.[7,8] AD-MWNTs have been shown to exhibit in their electronic transport properties if the diameter is sufficiently small (<20 nm), a clear division into semiconducting and metallic cases, which is much more obscured in CCVDs.[9]

Transmission electron microscope (TEM) images of MWNTs occasionally reveal an abruptly ending single layer within the multishell structure.[10] Especially, if a rupture happens to be in an outer layer, it is visible as a step with the height corresponding to the

intershell distance. A ruptured outer layer (or several layers) offers the possibility of nano- or microscale telescoping action, that is, the sliding of the inner layers in and out from the outer layers. For larger diameter nanotubes, this has to our knowledge been demonstrated solely in AD-MWNTs.[11,12] Similarly, intershell conductivity is a potentially much more interesting topic in AD-MWNTs, for example, because one can expect the question of commensurable or incommensurable adjacent shells[13] to be entirely relevant in these well-ordered tubes. AD-MWNTs, in particular, have the potential for a variety of engineered structures if one could introduce well defined local single defects into them, since the effect of such a local defect, e.g., to the electronic structure, is not obscured by other defects in the vicinity.

AD-MWNTs have then been studied to some extent but they typically include only one or two experimental techniques on a given batch. Therefore, an investigation that combines several techniques on individual tubes and enables us to firmly correlate between the different data types is to our knowledge still missing. Moreover, the characteristics of MWNTs with steps, resulting from broken outer layers have not been studied in connection with a general characterization of the MWNT quality. In this work, we have studied single AD-MWNTs with Raman spectroscopy, high-resolution scanning tunneling microscopy (STM), field-effect conductivity measurements, and nanomechanical probing with atomic force microscopy (AFM). The former two techniques probe the structural quality of the MWNT while the latter two the physical properties that depend on these qualities. We mainly study the nondefective cases but also some with a broken outer shell. Our results demonstrate the high quality of AD-MWNTs. Moreover, broken outer shells may be interesting engineering features in AD-MWNTs, as we show by measuring a distinct resistance over the step formed by them on the outer diameter of an AD-MWNT.

II. EXPERIMENT

AD-MWNTs were obtained from MER Corp. (USA) or Sigma-Aldrich. Another type was obtained from a collaborating group in Japan.[14] These contained amorphous carbon particles but no catalyst. A powder of the AD-MWNT material was dispersed in 1,2-dichloroethane, and the resultant suspension was sonicated for approximately 10 min. This dispersion was deposited via spin coating on the substrates. The substrate for MWNT deposition was Si/SiO_2. For the conductivity and Raman experiments, it had prefabricated marker structures. For the STM experiments, the substrate was Au/mica. In substrates with marker structures, selected MWNTs (as clean as possible) were located with respect to the markers with an AFM (Bruker Dimension 3100), which also was capable of detecting broken outer layers. For the conductivity measurements, two or more microelectrodes were fabricated on the selected individual MWNTs with conventional e-beam lithography. The microelectrodes (and associated bonding pads) consisted of a 2 nm thick sticking layer of titanium and approximately 30 nm of gold. For the nanomechanical experiments, on the Si/SiO_2 substrate multiple 200 nm deep, and a few hundred nanometers wide trenches were etched so that they covered a wide area of it. A few MWNTs could then be found that crossed at their middle section over the trench, which then was suspended.

For the STM studies, procedures that are common for these experiments were followed. Cleaved mica substrates were coated with an epitaxially grown 140 nm thick Au(111) film that was annealed at 530 °C, which produced a mesa-kind of structure with a locally atomically flat surface. Upon AD-MWNT deposition, such a density of deposited individual tubes was chosen, which would enable imaging them within the 1-μm scan range of the STM operating at low temperatures. Prior to STM measurements, the sample was annealed in ultrahigh vacuum (UHV) at temperatures of about 700 K to remove surface contamination due to exposure to ambient conditions.[15]

Resonant Raman spectra from individual AD-MWNTs, localized on the substrate with respect to the marker structures, were excited with an Ar ion laser (514 nm/2.41 eV) and recorded using a single monochromator Renishaw InVia Reflex spectrometer, equipped with a notch filter and CCD detector. All experiments were performed in the backscattering geometry under ambient conditions. A 100× microscope objective was used for focusing of the laser beam and collection of the scattered light. The laser spot had a diameter of ~1 μm at the sample with a power density of $\sim 10^6$ W/cm^2.

Three-terminal conductance measurements are performed by applying dc voltages (V_{DS}) from a voltage source (Yokogawa) to the AD-MWNT device electrodes and measuring the current (I) using a low noise current amplifier (Ithaco).[9] The samples were cooled to 4.2 K in a bath cryostat. The current was kept below 1 μA to avoid self-heating and damage to samples. A backgate voltage (V_G) is applied from a highly doped silicon substrate.

STM measurements are performed in a low-temperature UHV STM setup at temperatures of 78 K or 4.5 K (Omicron Nanotechnology, base pressure in the 10^{-11} mbar range). Operating the STM at cryogenic temperatures results in considerably more stable tunneling current and reduced thermal drifts. Electrochemically etched W tips that are cleaned *in situ*[16] are used. STM topographic imaging is performed in constant current mode. The bias voltages are applied to the sample while the STM tip is virtually grounded. Image processing was performed by Nanotec WSXM.[17]

We have previously developed an instrument that joins STM and AFM with electron microscopes.[18] Here, we have used the force sensor[19] inside a scanning electron microscope (SEM) in order to characterize the mechanical behavior of single MWNTs. The SEM is a LEO 1530 with a field emission gun and an optimum beam size of around 2 nm, which allows for accurate determinations of the nanotube diameters.[20] The force sensor was calibrated by pushing against a calibrated AFM cantilever from MikroMash, and the setup has been described previously in Ref. 21. Using the SEM, we are then able to position the force sensor over individual, suspended MWNTs, and measure their mechanical response.

III. RESULTS

A. Raman spectroscopy

Raman spectroscopy studies were performed on 27 individual AD-MWNTs having broad ranges of outer diameters (from 3.9 to 17.5 nm) and lengths (from 1 to 4 μm), estimated by the AFM technique. Overall, 19 nanotubes were in resonance at 514 nm excitation wavelength. Raman spectra for the most representative of

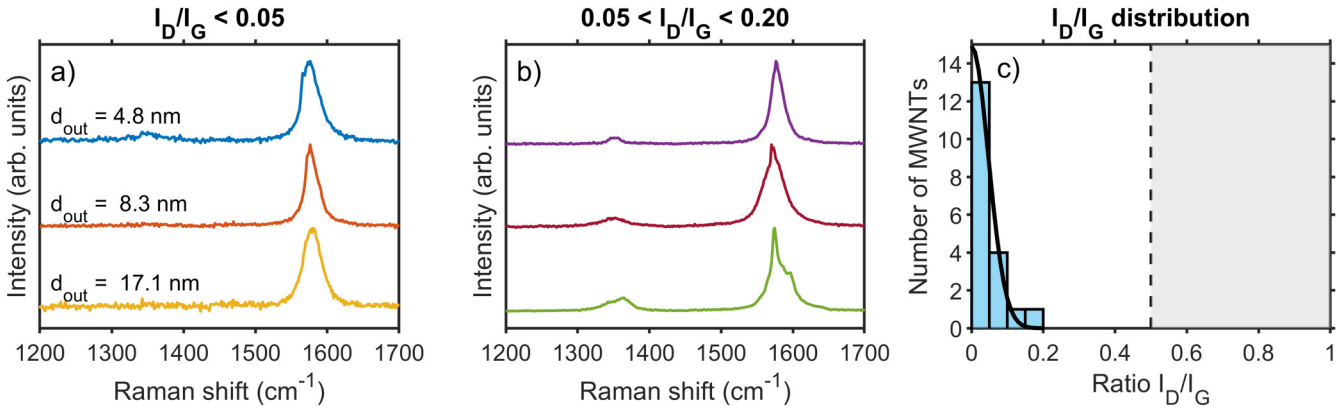

FIG. 1. D- and G-band ranges of Raman spectra measured at 514 nm excitation wavelength for (a) three individual AD-MWNTs with $I_D/I_G < 0.05$ and with outer diameters 4.8, 8.3, and 17.1 nm; (b) three individual AD-MWNTs with $0.05 < I_D/I_G < 0.20$; (c) experimental distribution for I_D/I_G values in the investigated AD-MWNTs. The Raman spectra of the most representative nanotubes from the first bin are shown in Fig. 1(a) while those from the second, third, and fourth bins are displayed in Fig. 1(b) from top to bottom, respectively. The gray area represents typical values for CCVD-MWNTs.

them are shown in Figs. 1(a) and 1(b) with the subtracted Si/SiO_2 substrate response. No radial breathing-like modes were detected at the given excitation wavelength (not shown). The intensity ratio I_D/I_G between the defect-induced D- and tangential G-modes is less than 0.05 for 13 out of 19 AD-MWNTs [Fig. 1(a)] while for the rest is lying in the range from 0.07 to 0.16 [Fig. 1(b)]. The experimental I_D/I_G distribution can be best fitted by the half-normal function, as illustrated in Fig. 1(c) by the black curve with the center at 0 and standard deviation $\sigma = 0.047$. The gray area in Fig. 1(c) represents typical values of I_D/I_G measured in CCVD-MWNTs.[22–24]

B. STM

The inset of Fig. 2 presents a typical example of a fragment of the STM topography image of an AD-MWNT with $d = 3.9 \pm 0.1$ nm deposited on an Au(111) surface. The main figure presents a high-resolution close-up view. Image processing [WSXM (Ref. 17)] is used to minimize the height variation related to the cylindrical curvature of the tube. This way, the height variations related to the atomic structure of the AD-MWNT can be better resolved. The technique described in Ref. 25 is used to determine the chiral indices of the outer shell of this AD-MWNT. The chiral indices are determined to be (33,24). According to this, the shell would be metallic. We note that practically all 17 obtained atomic resolution STM topography images of different AD-MWNTs do not reveal any defects in the atomic structure of their outer shells.

C. Nanomechanical measurements

The nanomechanical characterizations were performed on AD-MWNTs that were suspended over trenches in the Si/SiO_2-substrates, as shown in Fig. 3. The samples were first imaged perpendicular to the SEM beam in order to accurately determine the diameter and suspended length of the nanotubes. In order to image the very tip of the force sensor, the geometry was altered such that the SEM beam came in at a shallow angle toward the substrate while the sensor and sensor tip are moved perpendicular to the substrate during force curves. The inset of Fig. 3 shows an individual nanotube in contact with the force sensor. A typical force versus distance curve is shown in Fig. 4. The red curve (forward, color online) shows the very first force curve obtained from this nanotube while approaching the surface, and the blue curve (reverse, color online) is the retraction to the starting point. Though we will not in this article dwell more deeply in this, one

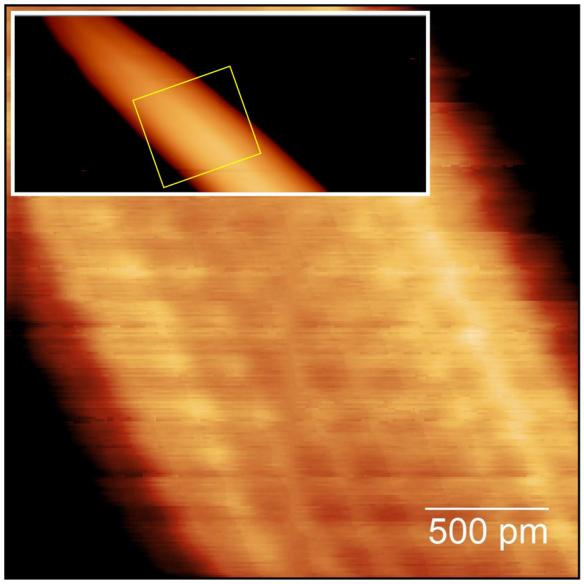

FIG. 2. STM image of an AD-MWNT acquired with atomic resolution. Inset: a larger scale STM image on which is indicated the region from which the main image was acquired.

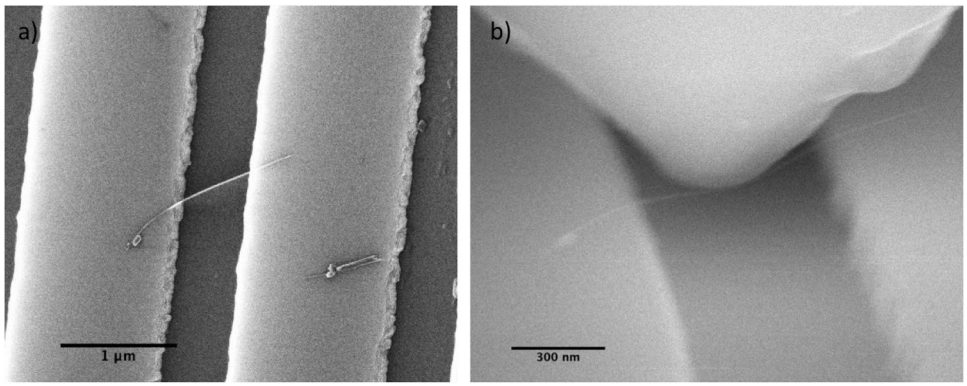

FIG. 3. (a) SEM image of the substrate with an individual nanotube bridging across one of the trenches in the sample (electron beam perpendicular to the substrate). (b) An SEM image of the force sensor in contact with the suspended nanotube [the same tube as in (a) but with the electron beam at a shallow angle to the substrate].

can in Fig. 4 identify several linear regions separated by abrupt drops in the force that appears when the nanotube slips against the sample.[26]

D. Conductance measurements

Figure 5(a) shows an AFM image of a typical single AD-MWNT with fabricated microelectrodes. The current versus gate voltage characteristics (I versus V_G or "gate curve") of the majority of the samples exhibit a slight transport gap already at room temperature, as we show later below in connection with Fig. 8. Upon cooling, the transport gap accentuates. In practice, all the samples have a maximum conductance at negative gate voltages.[9] Using the vocabulary of transistor devices, this corresponds to the minimum On-state resistance R_{MIN} of the device. In metallic or quasimetallic samples, though, the conductance variation is almost negligible. We have recorded the R_{MIN} of a large number of AD-MWNTs with different interelectrode spacings (L) and tube diameter (D), as is shown in Fig. 5(b). The figure shows R_{MIN} versus L, for different values of D, in the range of 2–8 nm.

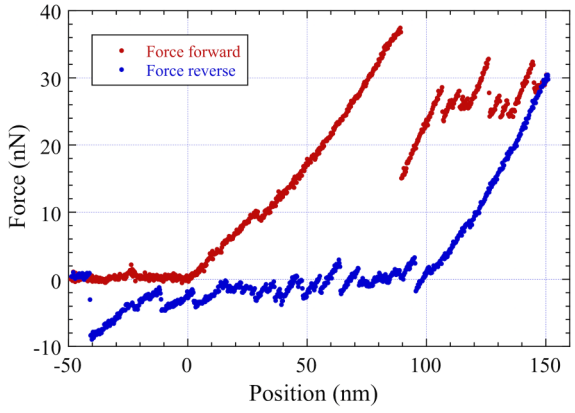

FIG. 4. Applied force versus the position of the force sensor during approach (red, left curve) and retraction (blue, right curve) from the surface.

AFM and STM images of AD-MWNTs reveal the occasional apparent step in the tubes from the material we use. An AFM image of an AD-MWNT with presumed one or more discontinuous outer layers is shown in Fig. 6(a). In turn, an STM image of a similar height discontinuity is shown in Fig. 7(a) with a much better accuracy. The rupture of an outer shell is visible as a step with the height corresponding to the intershell distance of 0.34 nm which is presented by the topography profile in Fig. 7(b).

We aimed to measure the resistance of the apparent step in the AD-MWNT in Fig. 6. For this purpose, the tube had four microelectrodes fabricated onto it so that the four electrodes divide it into three measurable sections called A, B, and C with the interelectrode spacing, L, around 0.75 μm (see the inset in Fig. 8). The middle section B contains the step while sections A and C measure over smooth sections but of slightly different diameter and then different shells to which the electrodes connect.

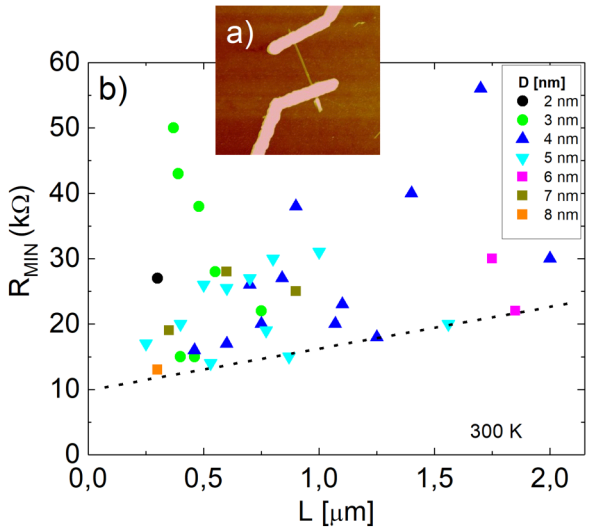

FIG. 5. (a) AFM image of MWNT with two electrodes (image size 2 μm). (b) Minimum on-state resistance R_{MIN} at 300 K, as a function of L and for different D, indicated in the inset. The dotted line is explained in the text.

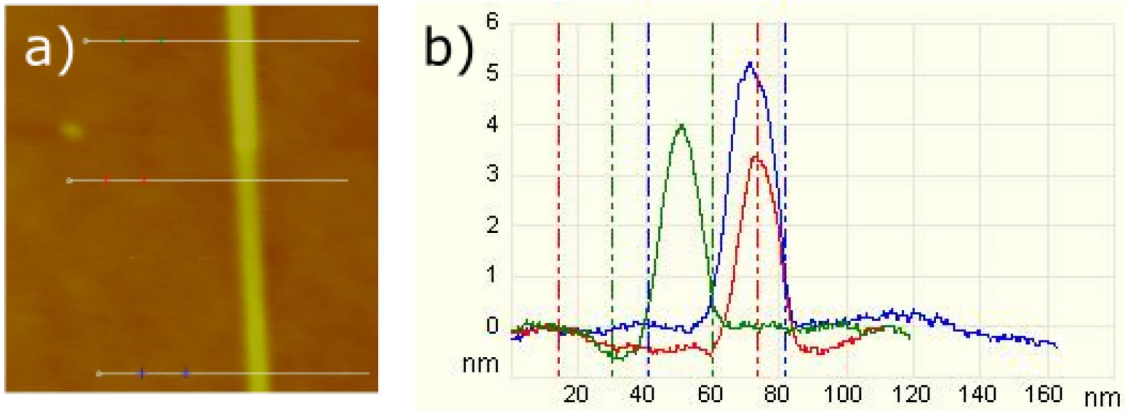

FIG. 6. (a) AFM image of an AD-MWNT section with a step. The step (and the thicker section) is just above the middle line. (b) Height profiles across the tube along the lines in the image (a).

Figure 8 shows conductance measurements across the three sections A, B, and C. The data include current I at constant bias voltage, and as a function of the gate voltage V_G, taken for each section at room temperature and at 4.2 K. In both cases, R_{MIN} is at the negative gate voltages, as we discussed earlier. The smooth sections A and C exhibit semiconducting behavior with transport gaps of different strengths. As expected, at lower temperatures, the transport gap becomes more prominent.

In section B, the behavior of the transport gap is intermediate between these two, but of main interest, in this case, is rather the ON-state resistance at both positive and negative gate voltages, which is almost an order of magnitude larger than in the other two sections.

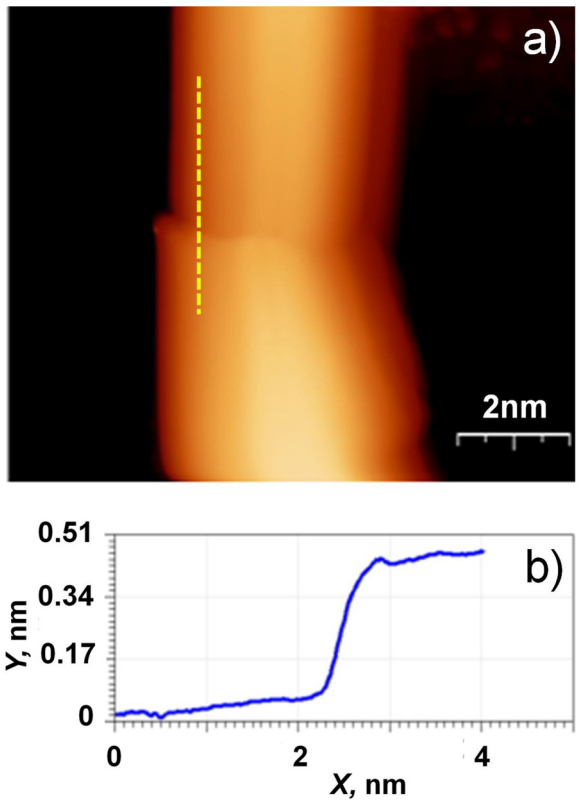

FIG. 7. (a) STM image of an AD-MWNT fragment with a discontinuous outer shell. (b) Height profile along the dashed line in (a).

IV. DISCUSSION

We can make rather immediate conclusions from the STM and Raman spectroscopy data. The STM data (Fig. 2 and other

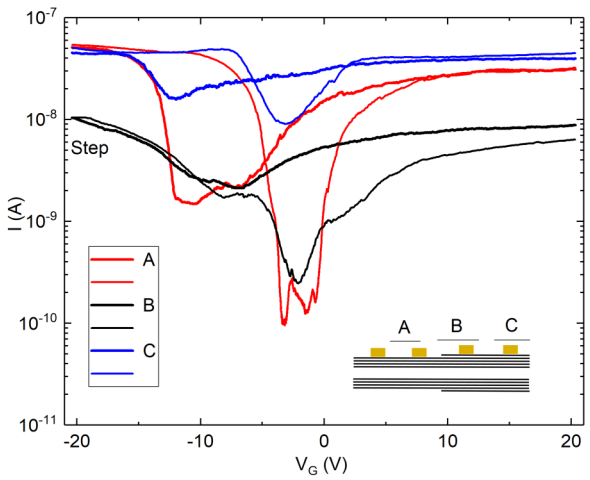

FIG. 8. Current (I) vs gate voltage (V_G) data of three different sections A, B, and C of the tube in Fig. 6(a), as is explained in the main text, and are schematically indicated in the insert in the lower right corner. Section B thus contains the step. The gate curves have been measured at room temperature and at 4.2 K. In each case, the 4K-curve is the one with a deeper transport gap.

samples) revealed a defect-free atomic structure of the outer layer of the AD-MWNT. In the Raman spectra, the D-band intensity, which is closely associated with the disorder, is small and is substantially lower than what was observed for CVD-grown MWNTs and MWNT bundles in the literature [I_D/I_G from 0.5 to 1 as shown by the gray area in Fig. 1(c)[22–24]].

The STM and Raman data give a direct measure of structural quality. In our case, the observations with these techniques point out a low density of defects and thus the high structural quality of the studied individual AD-MWNTs. The conductivity and nanomechanical measurements, on the other hand, should be a measure of the effect of the defectiveness on these properties. In other words, the low density of defects that the previous two measurement techniques imply would suggest values for the conductive and mechanical properties that are not too far from those expected for ideal MWNTs.

First, we look at the mechanical measurements. In order to obtain an estimate of Young's modulus from the force curve in Fig. 4 we need to make a few assumptions and simplifications regarding geometry and clamping. From SEM images, we find that the tubes are straight with long supports on both sides of the trench, we can then approximate the geometry as a double clamped beam without any pretension in the beam. The adhesion points are considered as fixed (up until the first slip), and we can use the slope of the first linear region in order to get an estimation of Young's modulus,[27] which provides a lower estimate of the modulus, as the clamping is not involving the whole circumference of the tubes.[28]

From the slope in the force curve in Fig. 4, we get an "effective" force constant (k_{eff}) that contains contributions from both the flexible force sensor (k_{tip}) and the nanotube (k_{CNT}). The contribution from the nanotube can be obtained from

$$k_{CNT} = \frac{k_{eff}}{1 - (k_{eff}/k_{tip})}. \quad (1)$$

Using the initial slope in the force curves and the nanotubes dimensions from SEM images, we then obtain an estimated Young's modulus value of about 460 ± 110 GPa. This value is much higher than what is typically seen in CVD-grown materials and is comparable to previous measurements of AD-MWNTs.[5]

The minimum resistance R_{MIN} at room temperature of a large number of samples is shown in Fig. 5(b), in which the data exhibits both diameter- and length-dependence. Devices with smaller D have a somewhat higher R_{MIN} at 300 K but overall the diameter dependence is rather small, which is consistent with the assumption of single-channel transport via the outer layer. The existing D-dependence is likely to be connected with a higher contact resistance, as the formation of reliable contacts becomes more challenging with decreasing tube diameter.

The R_{MIN} values range within 13–170 kΩ but most are closer to the dotted line, which indicates the lower boundary for R_{MIN} as a function of L. This line illustrates that R_{MIN} increases as the length L increases on the micrometer-scale. Electronic transport that occurs in one-dimensional channels have in the ballistic limit the quantized resistance for single shell carbon nanotubes as $h/4e^2 = 6.5$ kΩ.[13] In Fig. 5, the modest L dependence is indicated by the dotted line, which can be fitted to the formula,

$$R(L) = R_C + \rho L, \quad (2)$$

where $R_C = 10.0$ kΩ and $\rho = 6.4$ kΩ/μm. The formula expresses the resistance as composed of the contact resistance (R_C) and a one-dimensional resistivity (ρ). At $L = 0$, the line extrapolates to R_C which is only a little larger than the ballistic limit. The obtained value for ρ is similar to what is typically observed in "normally defective" SWNTs (Ref. 2) and compares reasonably well with reported values for AD-MWNTs.[29] The small resistance for most of the samples strongly suggests a small concentration of defects and a relatively large mean free path, on the order of a few 100 nm, even approaching the micrometer-scale. Thus, both the nanomechanical and the transport measurements indicate a high crystallinity of the material

Perhaps the most dramatic ramification of a high-quality MWNT is the telescopic action whereby one or more of the few outer layers are abruptly broken and the inner layers can slide out from the tube, as was mentioned in Sec. I. These experiments have (typically) been arranged with a micromanipulator that approaches in free space the free end of a single AD-MWNT, protruding from some substrate. With some extra effort, the interlayer resistance has also been measured, as both the substrate and the manipulator probe connection can be conductive.[11,12] However, this configuration has poor possibilities to include an efficient gate voltage coupling.

The interlayer conductance has also been measured with the conventional conductance measurement configuration shown in Fig. 5(a), on tubes with an intact shell structure and multiple electrodes connecting to the outer shell. To explain the idea, consider four consecutive electrodes labeled 1, 2, 3, and 4. Then, a voltage applied in electrode pair 1–2, can due to the extreme conductive anisotropy resulting from the shell structure (especially in AD-MWNTs), lead to a so-called nonlocal voltage arising in the electrode pair 3–4. With this method, Bourlon *et al.*[30] estimated an intershell resistivity of approximately 10 kΩ/μm in AD-MWNTs of diameter 17 nm.

To our knowledge, a measurement of the type demonstrated in Fig. 8 has not been reported previously. The R_{MIN} value for the sections on either side of the step, A and C, is around 20 kΩ. The R_{MIN} value for section B is around 100 kΩ that is about one order of magnitude larger than the value in the above mentioned work of Bourlon *et al.*, which most closely resembles our configuration. We consider this difference to be both consistent and interesting. Namely, the previous report involved an AD-MWNT of a much larger diameter (17 nm) than in our sample of diameter 4–5 nm. An intershell resistance that increases with decreasing diameter can be expected although theoretically, this detail is to our knowledge still a rather unexplored topic. Our results in this tedious experimental work so far only include this one sample.

V. SUMMARY AND CONCLUSIONS

We have performed various measurements on arc-discharge synthesized MWNTs that quantify their structural and the resulting physical properties from different angles. The results confirm the

high quality of this type of tubes and that their structure is reasonably close to the ideal picture of defect-free, concentric SWNTs. We have also studied the case of MWNTs with an abruptly broken outer layer. The interlayer conductance measurements over the step due to the broken outer layer enhance the viewpoint that in high-quality tubes certain local defect structures can be very useful.

ACKNOWLEDGMENTS

The authors thank D. Mtsuko for early contributions to this work. M.A. acknowledges the Academy of Finland for financial support. D.L. acknowledges financial support from the Russian Foundation for Basic Research (Grant No. 18-29-19043 mk).

REFERENCES

[1]S. Iijima, Nature **354**, 56 (1991).
[2]A. Jorio, M. Dresselhaus, and G. Dresselhaus, *Carbon Nanotubes* (Springer, Berlin, 2008).
[3]P. X. Hou, C. Liu, and H. M. Cheng, Carbon **46**, 2003 (2008).
[4]M. J. Hokkanen, S. Lautala, D. Shao, T. Turpeinen, J. Koivistoinen, and M. Ahlskog, Appl. Phys. A **122**, 634 (2016).
[5]H. Jackman, P. Krakhmalev, and K. Svensson, Appl. Phys. Lett. **104**, 021910 (2014).
[6]M. Flygare and K. Svensson, Today Commun. **18**, 39 (2019).
[7]J. M. Benoit, J. P. Buisson, O. Chauvet, C. Godon, and S. Lefrant, Phys. Rev. B **66**, 1 (2002).
[8]S. Nanot, M. Millot, B. Raquet, J. M. Broto, A. Magrez, and J. Gonzalez, Phys. E **42**, 2466 (2010).
[9]D. Mtsuko, A. Koshio, M. Yudasaka, S. Iijima, and M. Ahlskog, Phys. Rev. B **91**, 195426 (2015).
[10]J. H. Lehman, M. Terrones, E. Mansfield, K. E. Hurst, and V. Meunier, Carbon **49**, 2581 (2011).
[11]J. Cumings and A. Zettl, Phys. Rev. Lett. **93**, 086801 (2004).
[12]K. E. Moore, O. Cretu, M. Mitome, and D. Golberg, Carbon **107**, 225 (2016).
[13]J.-C. Charlier, X. Blase, and S. Roche, Rev. Mod. Phys. **79**, 677 (2007).
[14]A. Koshio, M. Yudasaka, and S. Iijima, Chem. Phys. Lett. **356**, 595 (2002).
[15]K. Schouteden, A. Volodin, D. A. Muzychenko, M. P. Chowdhury, A. Fonseca, and J. B. Nagy, Nanotechnology **21**, 485401 (2010).
[16]K. Schouteden and C. Van Haesendonck, Phys. Rev. Lett. **103**, 266805 (2009).
[17]I. Horcas, R. Fernandez, J. M. Gomez-Rodriguez, J. Colchero, J. Gomez-Herrero, and A. M. Baro, Rev. Sci. Instrum. **78**, 013705 (2007).
[18]K. Svensson, Y. Jompol, H. Olin, and E. Olsson, Rev. Sci. Instrum. **74**, 4945 (2003).
[19]A. Nafari, D. Karlen, C. Rusu, K. Svensson, H. Olin, and P. Enoksson, J. Microelectromech. Syst. **17**, 328 (2008).
[20]H. Jackman, P. Krakhmalev, and K. Svensson, Ultramicroscopy **124**, 35 (2013).
[21]H. Jackman, P. Krakhmalev, and K. Svensson, Appl. Phys. Lett. **98**, 183104 (2011).
[22]X. Yang *et al.*, J. Phys. Chem. C **119**, 27759 (2015).
[23]S. N. Bokova, E. D. Obraztsova, V. V. Grebenyukov, K. V. Elumeeva, A. V. Ishchenko, and V. L. Kuznetsov, Phys. Status Solidi B **247**, 2827 (2010).
[24]J. Judek, C. Jastrzebski, A. Malolepszy, M. Mazurkiewicz, L. Stobinski, and M. Zdrojek, Phys. Status Solidi A **209**, 313 (2012).
[25]L. C. Venema, V. Meunier, Ph Lambin, and C. Dekker, Phys. Rev. B **61**, 2991 (2000).
[26]K. McElroy, R. C. Davis, and A. Hawkins, Appl. Phys. Lett. **91**, 233119 (2007).
[27]J.-P. Salvetat *et al.*, Phys. Rev. Lett. **82**, 944 (1999).
[28]J. Zhang, Sci. Rep. **6**, 38974 (2016).
[29]B. Stojetz, C. Miko, L. Forro, and C. Strunk, Phys. Rev. Lett. **94**, 186802 (2005).
[30]B. Bourlon, C. Miko, L. Forro, D. C. Glattli, and A. Bachtold, Phys. Rev. Lett. **93**, 176806 (2004).